AGU PUBLICATIONS

JGR

Journal of Geophysical Research: Space Physics

RESEARCH ARTICLE
10.1002/2015JA021927

Effects of meteoric smoke particles on the *D* region ion chemistry

Carsten Baumann[1], Markus Rapp[1,2], Milla Anttila[1], Antti Kero[3], and Pekka T. Verronen[4]

[1]Deutsches Zentrum für Luft-und Raumfahrt, Institut für Physik der Atmosphäre, Oberpfaffenhofen, Germany, [2]Also at Meteorologisches Institut München, Ludwig-Maximilians-Universität München, Munich, Germany, [3]Sodankylä Geophysical Observatory, University of Oulu, Sodankylä, Finland, [4]Earth Observation, Finnish Meteorological Institute, Helsinki, Finland

Key Points:
- Ionospheric modeling of the *D* region ion chemistry including meteor smoke particles
- Diurnal variations of charged MSP number density and plasma composition differences
- Case studies during sunlit and dark conditions for the analysis of individual ion behavior

Correspondence to:
C. Baumann,
carsten.baumann@dlr.de

Citation:
Baumann, C., M. Rapp, M. Anttila, A. Kero, and P. T. Verronen (2015), Effects of meteoric smoke particles on the *D* region ion chemistry, *J. Geophys. Res. Space Physics*, *120*, doi:10.1002/2015JA021927.

Received 17 SEP 2015
Accepted 19 NOV 2015
Accepted article online 21 NOV 2015

Abstract This study focuses on meteor smoke particle (MSP) induced effects on the *D* region ion chemistry. Hereby, MSPs, represented with an 11 bin size distribution, have been included as an active component into the Sodankyä Ion and Neutral Chemistry model. By doing that, we model the diurnal variation of the negatively and positively charged MSPs as well as ions and the electron density under quiet ionospheric conditions. Two distinct points in time are studied in more detail, i.e., one for sunlit conditions (Solar zenith angle is 72°) and one for dark conditions (Solar zenith angle is 103°). We find nightly decrease of free electrons and negative ions, the positive ion density is enhanced at altitudes above 80 km and reduced below. During sunlit conditions the electron density is enhanced between 60 and 70 km altitude, while there is a reduction in negative and positive ions densities. In general, the MSP influence on the ion chemistry is caused by changes in the electron density. On the one hand, these changes occur due to nightly electron scavenging by MSPs resulting in a reduced electron-ion recombination. As a consequence positive ion density increase, especially water cluster ions are highly affected. On the other hand, the electron density is slightly increased during daytime by a MSP-related production due to solar radiation. Thus, more electrons attach to neutrals and short-lived negative ions increase in number density. The direct attachment of ions to MSPs is a minor process, but important for long living ions.

1. Introduction

Aerosol particles of meteoric origin play an important role in the mesosphere and coinciding *D* region ionosphere by influencing such diverse processes as the nucleation of mesospheric ice particles and the mesospheric water vapor distribution [e.g., *Rapp and Thomas*, 2006; *Friedrich and Rapp*, 2009, and references therein]. *Rosinski and Snow* [1961] proposed the existence of meteoric vapor converted into particulate form within the mesosphere and stratosphere. Later modeling studies showed that these meteor smoke particles (MSPs) are formed in the mesopause region [*Hunten et al.*, 1980] and are subject to atmospheric transport [*Megner et al.*, 2008]. These particles have been also studied by means of mass spectrometric in situ measurements [*Schulte and Arnold*, 1992] and other rocket-borne techniques [e.g., *Rapp et al.*, 2010], as well as by radar techniques [*Strelnikova et al.*, 2007] and by satellite measurements [*Hervig et al.*, 2009]. There are also more recent studies which have identified the most probable composition of MSPs to be found in the group of metal oxides (FeO, MgO) and metal hydroxides (FeOH, MgOH) [*Hervig et al.*, 2012; *Rapp et al.*, 2012]. An extensive review of meteoric metals in the mesosphere and the formation as well as composition of MSPs from a chemical point of view can be found in *Plane et al.* [2015].

Insights into the composition of the *D* region ionic components originates from rocket-borne measurements with cryogenically pumped mass spectrometers [e.g., *Narcisi and Bailey*, 1965; *Arnold and Krankowsky*, 1971] and laboratory experiments provide the knowledge on ionization processes, ion reactions, and electron-ion recombination [e.g., *Mitra*, 1981; *Pavlov*, 2014, and references therein]. Combining both, ionospheric models helped to unfold the complex gas phase ion chemistry of the *D* region [*Turunen et al.*, 1996; *Kazil et al.*, 2003; *Winkler et al.*, 2009]. However, these models do not yet consider the effects of MSPs in the ion chemistry.

This work concentrates on the influence of MSPs on the ion chemistry of the *D* region ionosphere. Recent rocket-borne studies suggested that the *D* region charge balance is significantly influenced by MSPs [*Friedrich et al.*, 2012]. The observations suggest that MSPs act as a sink for *D* region electrons leading to a depletion

that can be reconciled by simplified ionospheric modeling [*Baumann et al.*, 2013; *Asmus et al.*, 2015; *Plane et al.*, 2014]. In this manuscript, the influence of MSPs on the ion chemistry is studied in particular using the Sodankylä-Ion and Neutral Chemistry model [*Verronen et al.*, 2005; *Verronen*, 2006].

Here we study the diurnal variation of the charged MSP concentration and plasma concentration at high latitudes. This article is structured as follows: Section 2 describes the Sodankyä Ion and Neutral Chemistry (SIC) model and the incorporation of MSPs and their interaction with the charged species. Section 3 covers the influence of MSPs on the *D* region chemistry. Here the diurnal variations of the *D* region with the presence of MSPs is analyzed and two case studies are performed. Within these two case studies, the behavior of different positive and negative ion species in the presence of MSPs is investigated for dark and sunlit conditions in more detail. Section 3.3 covers a qualitative discussion of the uncertainties introduced by implementing MSP into the SIC model. The conclusions of this study are drawn in section 4.

2. Model and Methods

2.1. SIC Model

The present study uses the Sodankylä Ion and Neutral Chemistry (SIC) model which was originally only an ionospheric model [*Turunen et al.*, 1996]. We only show the basic principles of the current SIC model version here; a complete description is given elsewhere [*Verronen et al.*, 2005; *Verronen*, 2006].

The SIC model is a one-dimensional model with a coupled ion and neutral chemistry including vertical eddy transport of neutral species. Its chemical reaction scheme incorporates 43 positive ion species, 29 negative ion species, and 32 neutral species. The model derives the concentrations of all individual ion components and 15 of the 32 neutral components. The rest of the neutral components are kept constant at defined concentrations. That is, the NRLMSIS-00 model [*Picone et al.*, 2002] is used to set the neutral background atmosphere at the modeled geographical location.

The SIC model includes all known ionization sources, i.e., galactic cosmic rays (GCR), solar irradiance, and particle precipitation (electrons and protons). This study, however, focuses on for undisturbed ionospheric conditions. Therefore, the ionization by electron precipitation and proton precipitation is turned off. Figure 1 shows the basic concept of the SIC model including input parameters, the external models mentioned above and the main SIC modules and how these are interconnected within SIC.

Since the GCR ionizes the neutral atmosphere only at lower altitudes, the photoionization is the major source of ionization at altitudes above 50 km. SIC derives the photoionization rates for N_2, O_2, O, NO, and $O_2(^1\Delta_g)$ leading to the primary ions N^+, N_2^+, O^+, O_2^+, and NO^+. The solar spectrum is taken from the Solar Irradiance Platform (former SOLAR2000 [*Tobiska and Bouwer*, 2006]).

The primary ions react with the neutral background atmosphere to form secondary ions, e.g., H_3O^+ cluster ions and NO^+ cluster ions. The free electrons produced by the photoionization can attach to neutral species and build negative ions, e.g., O_2^-, Cl^-. This is the case below 80 km, where the atomic oxygen concentration is low enough to not significantly detach electrons from the negative ions.

In Figure 2 the number concentrations of positive and negative ions are shown for nighttime and daytime conditions. The nighttime NO^+ profile is shifted upward and has slightly lower number densities compared to the day time. Since Lyman α radiation scattered by the Earth's geocorona ionizes NO also during nighttime, there is a remnant of NO^+. This also shifts the maximum ionization altitude of NO^+ upward. In contrast, O_2^+ has a higher-ionization energy than the photon energy of Lyman α and nearly vanishes during nighttime by recombination with electrons. Reactions with these primary ions lead to the formation of cluster ions, e.g., $NO^+(H_2O)$ and $H^+(H_2O)_n$. Water cluster ions of the form $H^+(H_2O)_n$ are represented in the SIC model for up to $n = 8$.

Also, in the negative ion concentration there are changes from day to night, but they differ in detail from the behavior of the positive ions. Mainly the composition of the negative ions changes from sunlit to unlit times, but these absolute number densities are similar at daytime and nighttime. This difference has two reasons. First, there are no free electrons in the lower *D* region during nighttime which leads to a loss of O_2^-, one of the primary negative ions. Second, atomic oxygen also vanishes during night below 80 km due to the lack of sunlight (not shown). That leads to an increase of CO_3^- because the loss processes, i.e., electron photo detachment and collisional detachment with atomic oxygen, are weakened. HCO_3^- is converted into Cl^- by subsequent reactions.

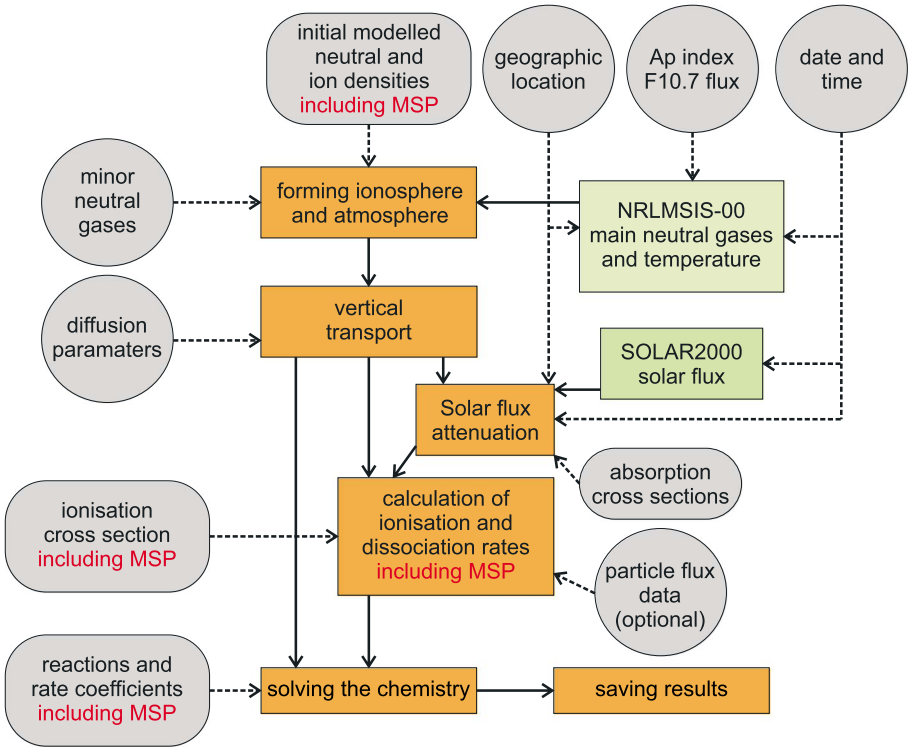

Figure 1. Schematic of the Sodankylä Ion Chemistry model, with input parameters, external models, and main SIC modules indicated by gray, green, and orange boxes, changes due to implementation of MSP is shown in red. Data input visualized by dashed lines, internal data handling is shown by solid lines, adapted from [*Verronen*, 2006, Figure 4.1].

2.2. MSP as a New Component

This section shows how MSPs have been implemented as an active component into the reaction scheme of the SIC model. Figure 1 indicates the modules and input parameters within the SIC model which have been adapted to achieve this implementation of MSPs. We have implemented four different processes involving MSPs into the SIC model. These are plasma attachment to neutral MSPs, recombination of charged MSPs with plasma, detachment of electrons from negatively charged MSPs and photoionization of neutral MSPs. Below, the derivation of the corresponding reaction rates is shown in detail.

In order to obtain size- and height-dependent information about the influence of MSPs on the *D* region ion chemistry, we included the MSP size distribution for different altitudes from the model of *Megner et al.* [2006]. The microphysical model of *Megner et al.* [2006] derives the concentrations of MSPs with sizes from 0.2 nm up to 40 nm for 30 to 100 km altitude. This microphysical model takes the meteoric mass input, the meteor ablation height, the vertical transport of MSPs by eddy transport, and the coagulation of MSPs into account. The size distribution has about 30 size bins when using the original model configuration. For practical reasons and to keep the SIC model stable, we have reduced this size distribution down to 11 size bins. Figure 3 shows this size distribution for an altitude of 90 and 60 km . At higher altitudes the number density of small particles is higher then the number of larger particles. That is because the MSPs are formed at ∼95 km. On their way down to lower altitudes the small particles sediment and coagulate to form bigger particles. Please note that the width of the size bins increase exponentially, i.e., the first bin has a width of 0.12 nm, while the eleventh bin has a width of 13 nm. These widths of the MSP size bins have been chosen due to the fact that the coagulation kernel of the underlying microphysical model requires such size bin widths.

The size distribution used does not consider horizontal transport as indicated by the study of *Megner et al.* [2008]. They made a transport experiment within their model scheme and identified the timescale of MSP transport from summer to winter pole induced by the meridional circulation to be in the order of 45 days. This horizontal transport is neglected in this study, since we only model the atmosphere for one single day. The time scale of meridional horizontal transport is thus much longer compared to the ionospheric processes which are subject of this study.

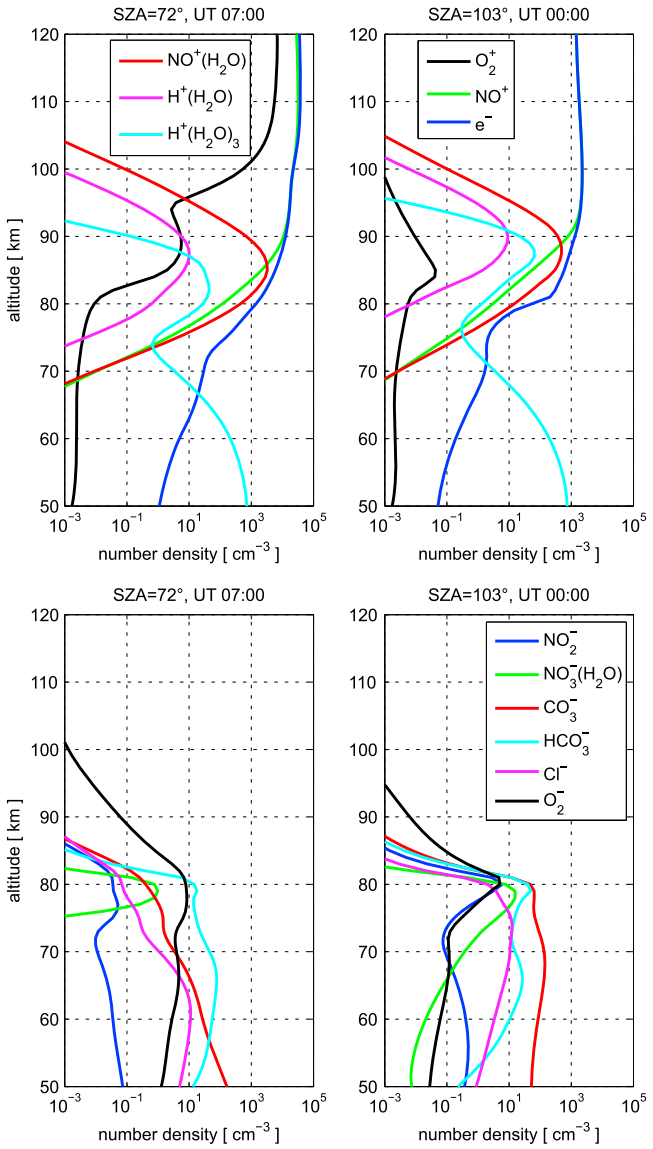

Figure 2. The number concentrations of the most abundant (top row) positive ions and (bottom row) negative ions for (left column) nighttime conditions and (right column) daytime conditions, SIC model results from 8 September 2010 for the location of Andenes (69°).

As a consequence of using 11 different MSP sizes the SIC model has been extended by 33 MSP components (neutral, singly charged positive, and singly charged negative MSPs). Reaction rates for charging and recombination of the MSP components with each plasma components are derived for all 11 MSP sizes. The reactions and corresponding reaction rates of MSPs with the plasma components are discussed in detail in *Baumann et al.* [2013, and references therein]. Nevertheless, we want to show the basic concepts of the involved processes and how they are included into the SIC model.

For the interaction of electrons and the individual ions with MSPs we apply the aerosol charging formalism of *Natanson* [1960] which has been adapted for mesospheric aerosols by *Rapp* [2000].

The charging process works as follows. The ion/electron attaches to a neutral MSP and is removed from the *D* region, i.e., the ion/electron is bound to the MSP and transfers the charge to it. The charging process of neutral MSPs is represented by the rate coefficient k_{charging} as follows:

$$k_{\text{charging}} = \gamma_{\text{charging}} \cdot \pi \cdot r_p^2 \cdot c_{e/i^+/i^-} \cdot \left(1 + \sqrt{\frac{e^2}{8 \cdot \epsilon_0 \cdot k_B \cdot T_{e/i^+/i^-}(h) \cdot r_p}}\right). \quad (1)$$

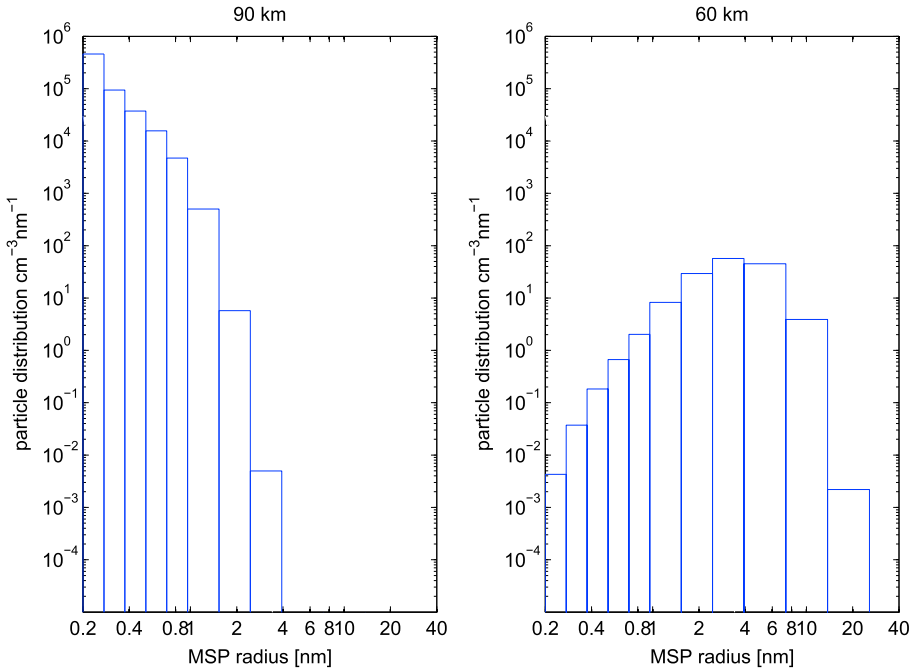

Figure 3. MSP size distribution for (left) 90 km altitude and (right) 60 km altitude, from the microphysics model of *Megner et al.* [2006] which represents September conditions in the Arctic.

The radius of the different MSP components is given by r_p; T is the temperature depending of the altitude h, which is the same for electrons and ions in the D region; ϵ_0 is the permittivity of free space; e is the elementary charge; and k_B is the Boltzmann constant. c represents the thermal velocity of the plasma components and is given by the formula $c_{e/i^+/i^-} = \sqrt{8kT/\pi m_{e/i^+/i^-}}$. Here $m_{e/i^+/i^-}$ is the mass of the positive (43 species), negative (29 species) ions and electron that can be captured by MSPs. Together with the 11 different MSP size components that leads to overall $(43 + 29 + 1) \cdot 11 = 803$ different reaction coefficients for the capture of plasma components. The dimensionless prefactor γ_{charging} represents a charging efficiency of particles by plasma components which is a function of particle size and composition. This charging efficiency γ_{charging} is not very well known and laboratory data for the expected MSP composition is not available. Nevertheless, *Megner and Gumbel* [2009] provide a valuable hint of this prefactors nature by analyzing laboratory data of the electron attachment efficiency of CO_2 and H_2O clusters [*Vostrikov and Dubov*, 2006a, 2006b]. We have adapted γ_{charging} from their Figure 6 in the following form:

$$\gamma_{\text{charging}}(r_p) = \begin{cases} 0, & \text{for } r_p < 0.25 \text{ nm}, \\ 0.8 \text{ nm}^{-1} \cdot r_p - 0.2, & \text{for } 0.25 \le r_p \le 1.5 \text{ nm}, \\ 1, & \text{for } r_p > 1 \text{ nm}. \end{cases} \quad (2)$$

Equation (1) represents the process where the plasma components induce an image charge within the MSP particle. That leads to an attractive force for the electrons and ions, i.e., the second term within the brackets. This attractive force leads to an increase of the thermal flow of plasma onto the surface of the MSP, i.e., the term of equation (1) before the brackets.

In this study the maximum charged state of a MSP is restricted to one elementary charge. Higher charged states of MSPs are possible, but the charging reaction rates of already charged particles are orders of magnitude lower because the Coulomb forces block off plasma from reaching the equally charged MSPs. In addition, *Rapp and Lübken* [2001] showed that particles with radii below 10 nm cannot carry charges bigger then one elementary charge at all.

When charged MSPs exist, it is also possible that these charged MSPs collect an oppositely charged plasma component. That process leads to a recombination of the charge carriers. Also, for this recombination

process, the ion/electron is bound to the charged MSP and is therefore removed from the *D* region. Equation (3) handles the recombination of charged MSPs with oppositely charged plasma components.

$$k_{\text{recomb}} = \gamma_{\text{recomb}} \cdot \pi \cdot r_p^2 \cdot c_{e/i^+/i^-} \cdot \left(1 + \frac{|q| \cdot e^2}{4 \cdot \pi \cdot \epsilon_0 \cdot k \cdot T_{e/i^+/-}(h) \cdot r_p}\right) \tag{3}$$

The difference between this equation and equation (1) is that direct Coulomb forces enhance the thermal flow of plasma onto the MSP surface. In addition to equation (1), q is here the absolute value of the charge number of the MSP.

The following recombination reactions can occur; electrons and negative ions can recombine with positively charged MSPs, and positive ions can recombine with negatively charged MSPs. These combinations again lead to 803 different reaction rates.

Finally, we have also implemented photo reactions of MSPs, namely, the photoionization of neutral MSP and the photo detachment of electrons from negatively charged MSPs. This means, these processes are an additional source of free electrons. By assuming a MSP composition of hematite (Fe_2O_3), photoreaction rates are derived after *Rapp* [2009].

$$k_{\text{photo}} = \int_0^{\lambda^*_{1/2}} F(\lambda, \chi, h) \cdot \sigma_{1/2}(r_p, n, Y_{1/2}, \lambda) \cdot \mathrm{d}\lambda. \tag{4}$$

Here F is the solar flux depending of the wavelength λ, solar zenith angle χ and altitude h, σ is the photoionization (1)/photodetachment (2) cross section for particles with radius r_p and the complex refractive index n, and Y is the photoemission yield. In practice, the lower wavelength limit is 100 nm as there is no available optical data of hematite for lower wavelengths. However, the solar flux is very low at these smaller wavelengths, so the contribution to the integral in equation (4) is negligible. The integration is ideally carried out from zero wavelength to a limit wavelength for the photoionization (λ^*_1), respectively, photodetachment (λ^*_2) process. The corresponding used photon energy for photoionization is 5 eV and for photodetachment 2 eV (see *Rapp* [2009] for discussion of these values). Photoionization and photodetachment reaction rates are derived for all 11 MSP sizes, leading to 22 MSP photoreactions. The solar flux data used for integration of equation (4) is given directly by the SIC model which uses the SOLAR2000 model data. The SIC model takes the attenuation of the solar flux within the atmosphere into account. For that, SIC derives the absorption of solar photons by the main components of the atmosphere and some minor species which are photoionized or photodissociated, i.e., O_2, N_2, O, Ar, He, NO, $O_2(^1\Delta_g)$, CO_2, O_3, NO_2, H_2O, H_2O_2, HNO_3, N_2O_5, and HNO_2. This derivation of the atmospheric attenuation results in the remaining solar flux corresponding to each modeled altitude bin.

All in all, 1628 reactions have been added to the SIC reaction scheme in order to implement 11 MSP size bins, which are derived for each modeled altitude bin. This already outnumbers the originally implemented reactions. The error introduced by the 11 bin size distribution is small since all relevant particle sizes (<10 nm) are well represented.

3. MSP Influence on Ion Chemistry

To study the effects of MSPs on the *D* region ion chemistry, we have performed two SIC model runs. One model run has been setup including MSPs and the corresponding reactions as described in section 2.2, i.e., the MSP-SIC run. The other SIC run uses the original reaction scheme and the MSP concentrations are set to zero, i.e., the standard SIC run . By doing that we can identify changes within the ion chemistry that are induced by the presence of MSPs. Both model runs represent quiet ionospheric conditions, i.e., with only solar radiation as ionization source, for high latitudes and September conditions. The correct functioning of the MSP-SIC model has been validated by comparing charge balance results with the simple ionospheric model of *Baumann et al.* [2013]. In addition, we have performed MSP-SIC model runs with different time stepping (not shown) which show identical results.

We present model results of a complete day to study the diurnal variation of the charged MSP species and their influence on the ion species and the free electron concentration in the polar *D* region ionosphere. After that two individual case studies are discussed in further detail. Here the effects of MSPs on specific ion concentration and the associated chemical processes are analyzed in detail for night (solar zenith angle (SZA) = 103°) and day (SZA = 72°).

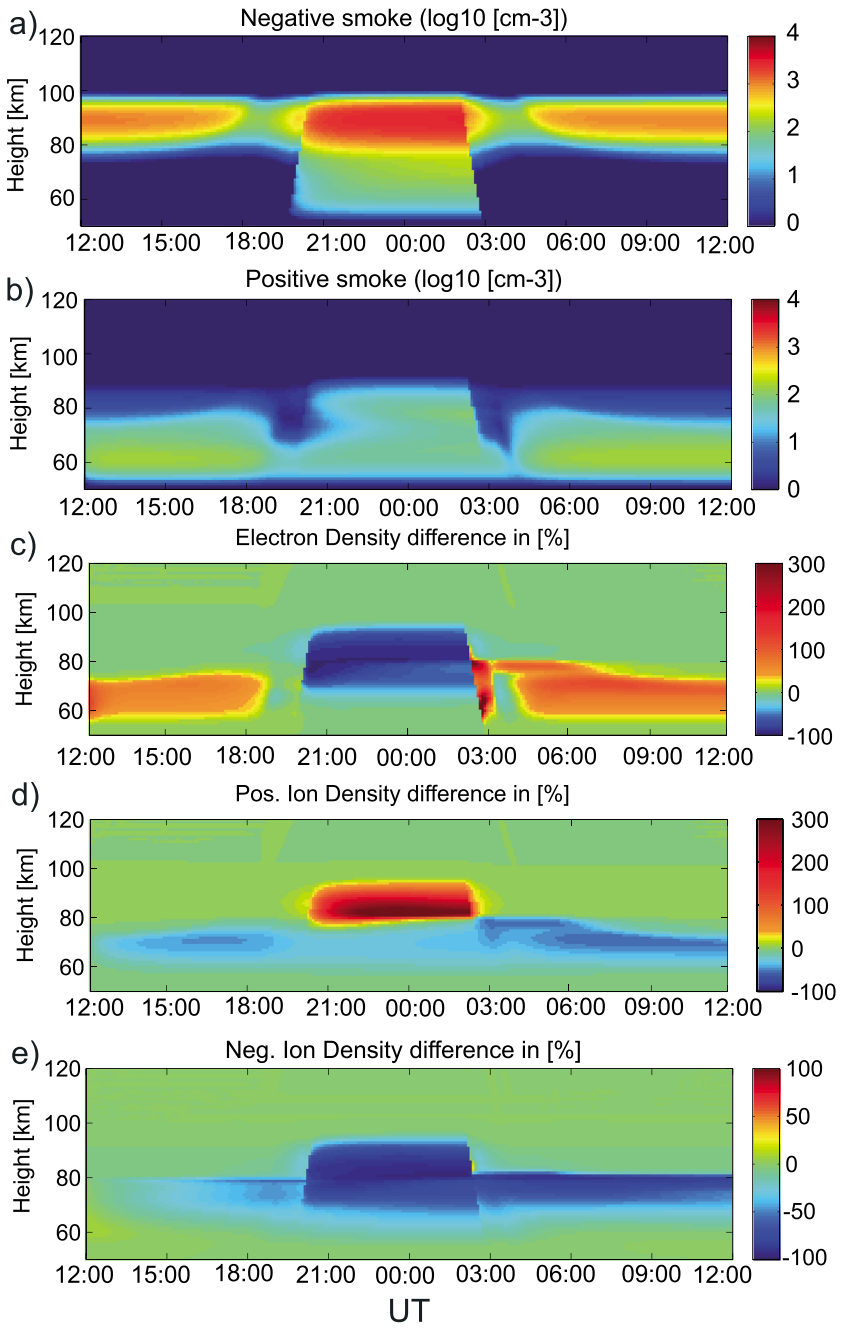

Figure 4. Diurnal Variation of the (a) negative MSP and (b) positive MSP, also shown are the diurnal variations of the (c) relative difference between a standard SIC model run and the SIC run with MSP for the electrons, (d) positive, and (e) negative ions.

3.1. Diurnal Variation

This section discusses the diurnal variations of negatively and positively charged meteoric smoke, as well as the relative differences between the MSP-SIC and standard SIC model runs of the electron density, of the sum of all positive ion concentrations and of the sum of all negative ion concentrations. Since the model has a time resolution of 5 min, the terminator appears as steps in the MSP densities as well as in the relative differences of the plasma.

At first we want to discuss the negatively charged MSP concentrations. Figure 4a shows a more or less continuous layer of negative MSPs between 80 and 100 km altitude. There are number densities of ~1000 cm^{-3} during daytime that are reduced during dusk and dawn down to several 100 cm^{-3} and after that increases

slightly again. Only during nighttime, when the Sun is far enough below the horizon so that the *D* region is not sunlit anymore, the negative MSP layer expands down to ~55 km altitude. For example, at 60 km altitude negative MSP number densities of 100 cm^{-3} exist. Electron attachment to neutral MSPs is very effective in the nighttime *D* region [*Baumann et al.*, 2013, and references therein].

The positively charged MSP abundance shows different characteristics as those of the negative one. There is a distinct layer of positive MSPs at lower altitudes, namely, between 55 and 75 km (see Figure 4b). Number densities of up to several 100 cm^{-3} exist during daytime. Similar to the negative MSPs the positive MSP layer is slightly reduced during dusk and dawn. During nighttime the layer expands up to 90 km with number densities of about 100 cm^{-3}.

It has to be noted that the coexistence of negatively charged MSPs and positively charged MSPs at the same time in the same altitude during nighttime has been measured by rocket-borne electrostatic deflection methods of *Robertson et al.* [2013]. Also, the dominance of positive MSPs at lower altitudes compared to the negative MSPs during daytime was shown in this study and hence supports our model results. However, the modeled ionospheric conditions do not match the exact conditions during the measurements.

Now, we want to consider the changes of the ions and electrons due to the presence of MSPs. Figures 4c–4e show the relative difference between the MSP-SIC and the standard SIC model of electrons, positive ions, and negative ions. Please note that the difference of the sum of all positive and all negative ion model species between both model runs is shown here.

The electron difference shows a very strong diurnal variation. During sunlit times there is a 60 to 100% enhancement of free electrons between 55 and 75 km, which coincides with the layer of positively charged MSPs at that time. The only possible explanation is MSP photoreactions, most likely photoionization, which is an additional source of free electrons. During dusk the electron enhancement nearly vanishes. At this time the optical path of solar photons within the atmosphere is greatly enhanced, which leads to the absorption (O_2, N_2) of photons with energies higher than 5 eV. Just after sunset in the *D* region (~20:00 UT) the electron relative difference drops down to −80%, indicating an effective electron attachment to neutral MSPs. This electron reduction expands to the altitude region between 70 and 95 km, which is not the complete layer thickness of negative MSPs during dark conditions. After sunrise (~3:00 UT) the electron reduction turns immediately into an enhancement of up to 300%. This enhancement has its origin in the electron photodetachment from negative MSPs. A similar effect of immediate photodetachment of electrons just after sunrise has been discussed by, e.g., *Kazil* [2002] for the negative ions. In both cases the argument of a too long optical path of solar photons during sunrise does not hold, since also photons with much lower energy can detach electrons. These low-energy photons, which are in the visible part of the solar spectrum, are hardly absorbed by the atmosphere and their solar flux is much higher than the UV photons with energies above 5 eV.

The influence of MSPs on the positive ion concentration is especially pronounced during nighttime. At this time there is an enhancement of positive ions for the MSP-SIC run compared to the standard SIC which reaches ~300%. This large enhancement can be explained by the reduced electron-ion recombination rate [*Rapp and Lübken*, 2001]. This rate is greatly reduced due to the electron scavenging by the neutral MSPs. During daytime the positive ion density is marginally affected by MSPs. At altitudes 70±10 km the ion concentrations are reduced by 20 to 40%, which is mainly due to the increased electron-ion recombination rate caused by the free electron enhancement here.

Negative ions are also affected by MSPs. Since negative ions only exist below ~80 km (compare Figure 2), effects shown as relative differences are only relevant below that altitude. Figure 4e shows a ~50% reduction in negative ion density over the complete day. During daytime the reduction is located from 80 km down to 65 km. This reduction occurs despite the fact that the electron density is enhanced at lower altitudes during sunlit times. After sunset the loss of negative ions extend to higher altitudes. In practice there is no negative ion species of relevant number density, so that these relative changes have no physical meaning above 80 km. This reduction is related to the attachment of negative ion species to neutral and positively charged MSPs. Also, the reduced abundance of free electrons during nighttime leads to lower production rates of negative ions.

In this section we only focus on the relative change in the sum of each positive and negative ions. The behavior of individual ions can differ significantly from the overall change of the sum of ions. Therefore, the next section discusses case studies to identify the chemical processes affected by the presence of MSPs.

3.2. Case Studies of Individual Ions

This section examines the influence of MSPs on groups of individual positive and negative ions for night (SZA = 103°) and day (SZA = 72°) conditions. The discussion of all individual ion components exceeds the scope of this article. Therefore, we choose ion species which show relevant changes, i.e., relative changes are bigger then 10% and the absolute abundance of the species is higher than 1 cm^{-3} in the *D* region. The ion species chosen also play an important role within the *D* region ionosphere [*Ferguson*, 1979].

The positive ions considered here are NO^+, $NO^+(H_2O)$, and $H^+(H_2O)_n$. These ions are connected by the following reactions:

$$NO + h\nu \rightarrow NO^+ + e^- \quad (5)$$

$$NO^+ + H_2O + M \rightarrow NO^+(H_2O) + M \quad (6)$$

$$NO^+(H_2O) + HO_x \rightarrow H^+(H_2O) + NO_{x+1} \quad (7)$$

NO is ionized by sunlight (5), then NO^+ can attach a water molecule (6). This water cluster can then react with a HO_x component to build positive water cluster ions (7).

These water cluster ions can grow by attaching additional water molecules in a trimolecular reaction (8). There is also a collisional loss process which reduces the attached water molecules. The reaction rates of this reaction have been quantified by *Lau et al.* [1982].

$$H^+(H_2O)_n + H_2O + M \rightarrow H^+(H_2O)_{n+1} + M \quad (8)$$

$$H^+(H_2O)_n + M \rightarrow H^+(H_2O)_{n-1} + H_2O + M \quad (9)$$

The SIC model represents water clusters with ligand numbers of up to eight. In the interpretation of our results we will focus on water cluster ions with one, three, and five ligands. Water cluster ions with higher ligand number do not exist at reasonable number densities.

The species O_2^-, Cl^-, and $Cl^-(HCl)$ are considered for the negative ion species, which are connected via a reaction chain. The reaction rates can be found in *Phelps* [1969] and *Kazil* [2002, and references therein].

$$O_2 + N_2 + e^- \rightarrow O_2^- + N_2 \quad (10)$$

$$O_2^- + HCl \rightarrow Cl^- + HO_2 \quad (11)$$

$$Cl^- + HCl + M \rightarrow Cl^-(HCl) + M \quad (12)$$

O_2^- is a primary negative ion, which is build by a trimolecular reaction with N_2 or O_2, i.e., neutral air. The Cl^- ion has many sources in addition to reaction (11). $Cl^-(HCl)$ is generated by the attachment of an additional HCl molecule to the Cl^- ion (12). The ion $Cl^-(HCl)$ is very long lived, since its only loss process ,except attachment/recombination with MSPs, is the detachment of HCl ligand in a reaction with O2/N2 (back reaction of (12)). This is also indicated by its high number density at lower altitudes. It has to be noted that the negative ion chemistry is, in general, more entangled compared to the positive ion chemistry.

3.2.1. Night Conditions

This section discusses the ion chemistry during nighttime conditions (SZA = 103°, 00:00 UT). Figure 5 shows the charge balance (top), individual positive ion number density (middle), and negative ion number density (bottom). As seen in experimental data [*Friedrich et al.*, 2012] and model data [*Baumann et al.*, 2013; *Asmus et al.*, 2015] the charge balance is kept between 80 and 95 km by negative MSPs. This is represented in this study too. Here negative MSP densities equal the positive ion densities around absolute values of 3000 cm^{-3}. Below ~80 km positive and negative MSPs tend to match up at number densities below 100 cm^{-3}.

When looking at the individual positive ions, one first notices that bigger ions exist at consequently lower altitudes. The highest number density of NO^+ occur at 95 km and above. In the MSP-SIC model run the number density shows a peak at 92 km at ~2500 cm^{-3}. Also, for the daughter ions of NO^+ the number densities are higher in the MSP model run compared to the standard SIC model run. This exceeds down to ~80 km, where

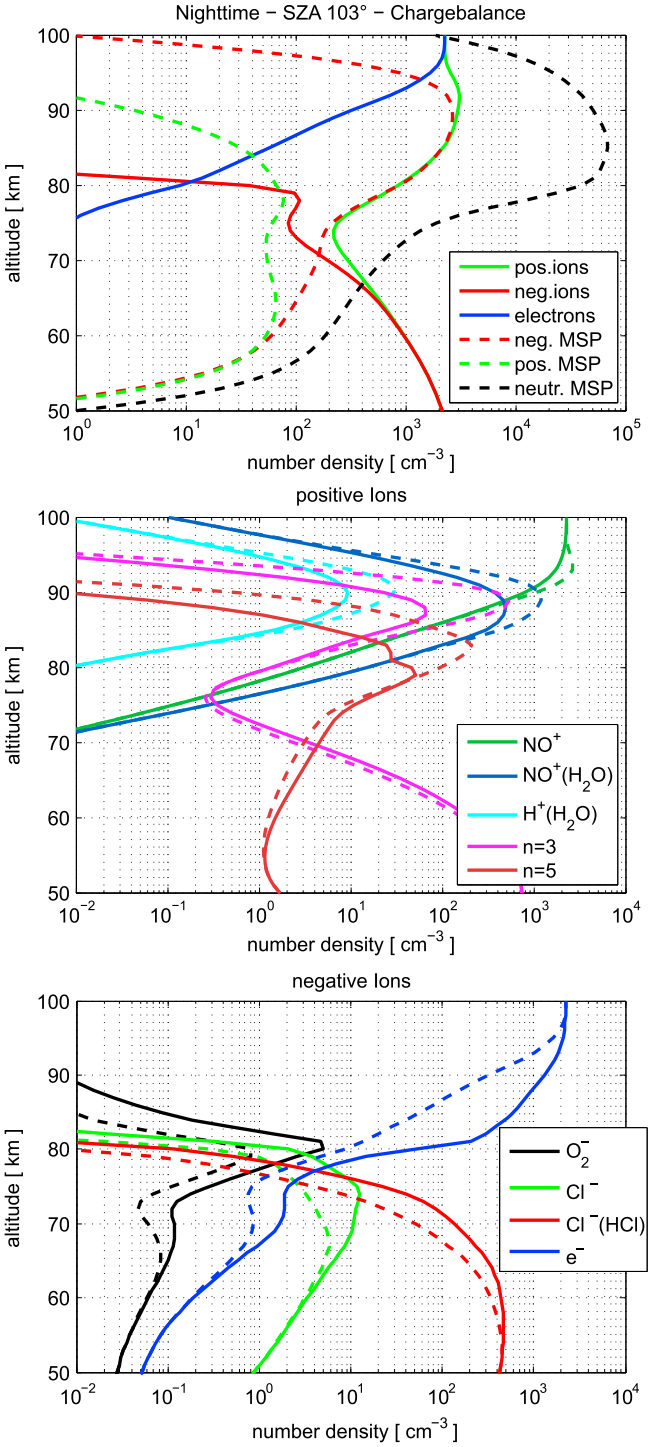

Figure 5. (top) The *D* region charge balance during 103° SZA with electron density and sum of all positive and negative ion concentration (solid) as well as sum of charged and neutral MSPs components shown (dashed) for the MSP-SIC model run, (middle) relevant positive ion concentration for the standard SIC run (solid lines) and the MSP-SIC run (dashed lines), and (bottom) relevant negative ion density and electron density.

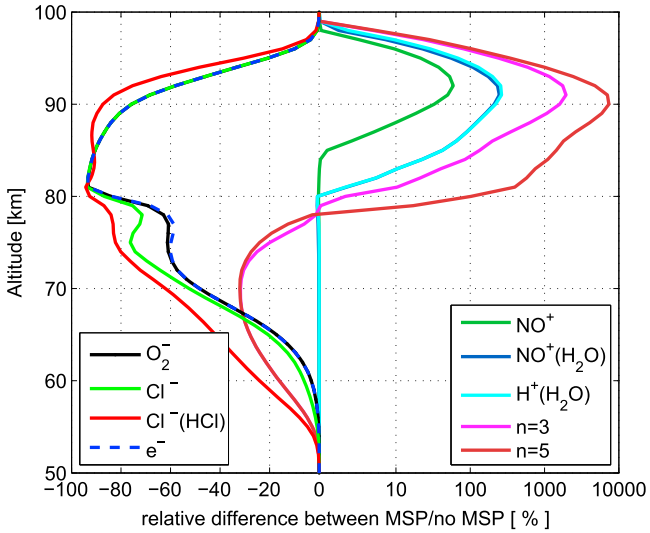

Figure 6. Relative difference of the ion and electron concentrations shown in Figure 5 between the standard SIC run and the MSP-SIC run for an SZA of 103°. Please note the logarithmic scale for the positive relative differences.

the excess of positive ions turns into a reduction of positive ions. Here the water cluster ions with ligand number higher than one are still abundant in reasonable number densities and can attach to neutral MSPs.

Negative ions exist only below 80 km, differences between the MSP-SIC run and the standard SIC model run are only visible here. The number densities of O_2^- and Cl^- are reduced down to 65km, while the reduction of $CL^-(HCl)$ expands down to 55 km. O_2^- and Cl^- show a similar behavior as the electron density , all of them drop in number density at lower altitudes. Only $Cl^-(HCl)$ is still abundant at number densities of several 100 cm^{-3}.

To give a quantification of the processes influenced by MSPs, Figure 6 shows the relative differences between the MSP model run and the standard model run of all above discussed species in one panel. The electron density is strongly reduced in the MSP case, which is the main cause for the changes in negative and positive ion chemistry. In the first place, the electron scavenging reduces the electron-ion recombination as well as the production of negative ions by electron attachment to neutral species. Since the electron-ion recombination is reduced down to 80 km, additional positive ion can exist here. The enhancement is rather small for NO^+ with 50%, which reacts fast with other neutral components to build secondary positive ions, but the enhancement of the positive ion density increases with ion size. The maximal enhancement for $NO^+(H_2O)$ and $H^+(H_2O)$ is 250%, grows for $H^+(H_2O)_3$ to 2000%, and even raises to 7300% for $H^+(H_2O)_5$. This successive growth of the water clusters is supported by the lacking electron-ion recombination, which is the main loss process for this group of ions. Only reaction (9) also reduces the growth of water cluster ions but is only of minor importance. Below 80 km, electron-ion recombination is not an important process in both model runs, i.e., the absolute density of free electrons is very low here. At these altitude only water cluster ions can still exist at reasonable number densities and are attached to neutral/negative MSPs resulting in their reduction of 30%.

The change of negative ions is also strongly influenced by the nightly loss of electrons. The relative change of the primary ion O_2^- is nearly identical to the electron relative change. This is because the O_2^- production by electron attachment to O_2 is much faster than the O_2^- loss by O_2 attachment to MSP. This is no more the case for the relative changes of Cl^- and $Cl^-(HCl)$. Cl^- shows a higher reduction between 70 and 80 km and $Cl^-(HCl)$ reduction is higher in the complete altitude region compared to the relative change of the electron density. This additional reduction of both ion species has its origin in their attachment to MSPs. In addition, the lack of free electron prevents the effective neutralization of positive MSP, which can exist at reasonable number densities. The recombination of positively charged MSP with negative ions is here an additional sink.

3.2.2. Day Conditions

This section discusses the ion chemistry during day time conditions (SZA = 72°, 07:00 UT). Figure 7 shows the charge balance (top), individual positive ion number density (middle), and negative ion number density (bottom) for this time.

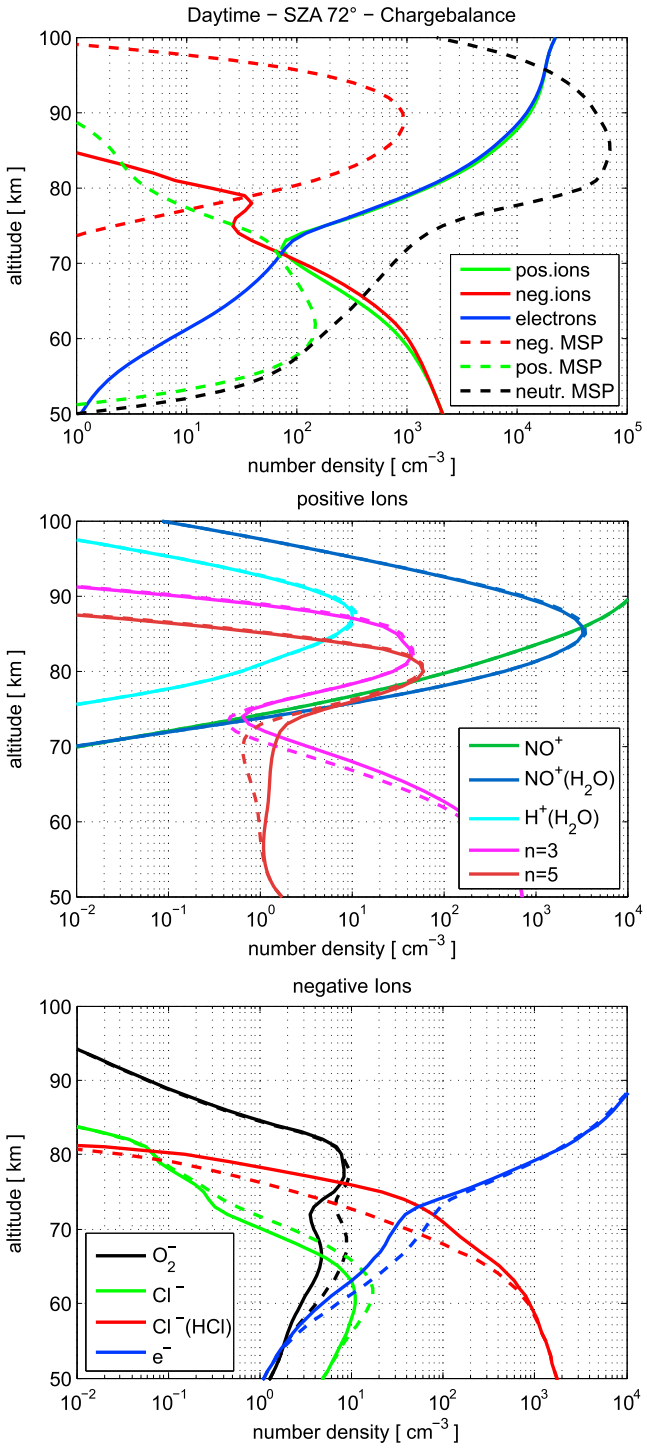

Figure 7. (top) Charge balance of the MSP-SIC run, (middle) positive ion, and (bottom) negative ion density as in Figure 5 but for an SZA of 72°.

The charge balance during sunlit condition is only slightly influenced by the presence of MSPs. Due to the photodetachment of negative MSPs, which balances the electron attachment rate, negative MSP abundance is only 1000 cm^{-3} at 90 km despite the 1 order of magnitude higher electron density compared to the nighttime case. Because of the now effective photodetachment in sunlit conditions, the presence of MSPs does not lead to an effective scavenging of electrons anymore. The photodetachment is so effective that below 75 km negative MSPs do not exist any longer. Moreover, shortwave solar radiation makes photoionization of MSPs

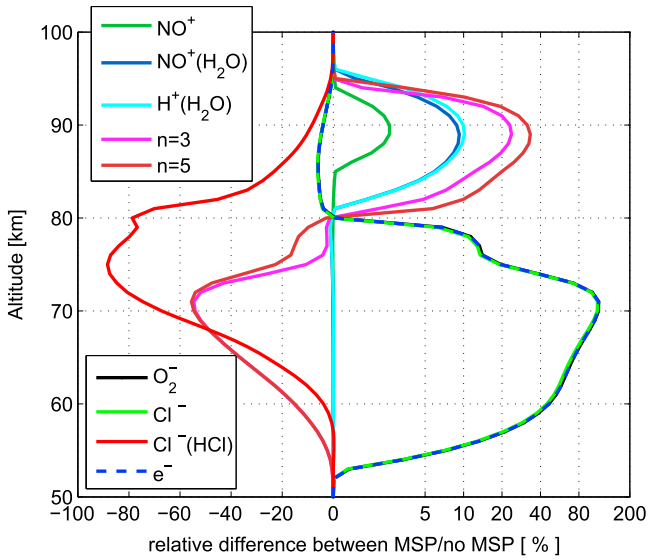

Figure 8. Relative difference of the individual ion and electron concentrations shown in Figures 5b and 5c between the standard SIC run and the MSP-SIC run for an SZA of 72°. Please note the logarithmic scale for the positive relative differences.

possible, which leads to a number density of positively charged MSP in the order of 150 cm^{-3} at 60 km. As a result, there are localized layers of negative MSPs (90 km) and positive MSPs (60 km). To some extent this is even represented in the measurements of *Robertson et al.* [2013], despite the fact that the measurement were made under disturbed ionospheric conditions while the model represents quiet conditions only.

Since negative MSPs are only marginally involved in the charge balance , electron density does not change significantly above 80 km. Consequently, the positive ion chemistry does not change due to the presence of MSPs. Below 80 km, the water cluster ions with ligand number 3 and 5, which are still abundant there, exist at lower number densities. The electron density is enhanced in this height region, which can only be explained by the photoionization of neutral MSPs. This higher abundance of free electrons leads to an increase of O_2^- production, which in turn also build more Cl^- ions. However, this enhancement does not pass over to the $Cl^-(HCl)$ concentration. On the contrary, $Cl^-(HCl)$ is similarly reduced as during nighttime.

Identically to the night time case study, Figure 8 shows the relative differences between the MSP-SIC model run and the standard SIC model run for all above shown positive and negative ions for sunlit conditions. The electron density is reduced by 10% at 90 km and enhanced by up to 120% below 80 km. Both changes can be accounted to MSPs directly. The electron loss is due to electron attachment to neutral MSPs, the effect is rather small due to effective photodetachment. The enhancement occurs due to free electron production by photoionization of neutral MSPs.

The daytime behavior of the electrons is as important as during the nighttime case. The minor reduction of electrons above 80 km increases the number densities of the positive ions in the same manner. The increase of NO^+ is below 5%, but the abundance of $NO^+(H_2O)$ and $H^+(H_2O)_{1/3/5}$ rises consequently with number of water ligands and is ~30% for $H^+(H_2O)_5$. The same argumentation as in the nighttime case is also valid during daytime, i.e., reduced electron-ion recombination enhances the number densities of positive ions. Below 80 km the electron density is at higher levels increasing the electron ion recombination in this altitude region. As a consequence, the number density of water cluster ions reduces to 50% of its original value, which means an additional reduction of 20% compared to the nighttime case, where only ion attachment to neutral particles is important.

Negative ions are also affected by MSPs during daytime and the major driver of this change is the electron density, as it is for the positive ions. While O_2^- and Cl^- difference directly follows the difference of electrons, the difference of $Cl^-(HCl)$ is completely decoupled from the electrons. The behavior of $Cl^-(HCl)$ is only governed by the attachment to neutral and recombination positive MSPs since it is such a long-lived ionic species. Both reaction rates are comparable to the only loss process of $Cl^-(HCl)$(back reaction of (12)), because an excess of

positive MSPs exists during daytime. The more short-lived species O_2^- and Cl^- are completely coupled to the electron density which indicates that their attachment to MSPs is not significant here. It has to be noted that there are also negative ion species that show a slightly different behavior. These species follow the electron governed behavior of O_2^- at higher altitudes and follow the MSP governed behavior of $Cl^-(HCl)$ at lower altitudes (not shown).

3.3. Discussion of Model Uncertainties

By implementing MSPs as an active component into the scheme of the SIC model we have introduced additional uncertainties into the model. These uncertainties originate from the microphysical and photoelectrical properties of MSPs which are not well known. The microphysical properties of MSPs are variables within the processes that link the *D* region ionosphere to MSPs (shown in section 2.2). This section covers a qualitative discussion of variable uncertainties and of their impact on the model results. Namely, the charging of MSPs and their photoelectric properties, the MSP number density and its size distribution itself as well as the influence of disturbed ionospheric conditions.

The charging of nanometer-sized MSPs by attachment of plasma was derived on the basis of classical electrodynamics [*Natanson*, 1960; *Rapp*, 2000], not taking into account quantum mechanical size effects. *Plane et al.* [2014] derived reaction rates from unimolecular kinetic theory for the electron attachment to a 0.25 nm MSP analog and found a good agreement to the rates derived by the classical formalism which is used in this study. However, the exact nature of the size dependent charging efficiency $\gamma_{charging}$ is still unknown. As shown in an above section we have used a representation of this charging efficiency introduced by *Megner and Gumbel* [2009] who rely on laboratory measurements of water and carbon dioxide nanoparticles. This representation of $\gamma_{charging}$ avoids the charging of the smallest (0.2 nm) MSPs by attachment of plasma components. This is reasonable, since allowing all MSPs to be charged would remove all free electrons from the *D* region which is not the case in reality. On the other hand, when increasing the charging threshold to larger MSP sizes reduces the influence of MSPs on the *D* region as they become increasingly inactive.

Other important variables in our model study are the photoelectric properties of MSPs. We used the work-function, electron affinity, and complex refractive index of hematite (Fe_2O_3) to derive the photoionization and photodetachment rates. In the case of higher electron affinities and work function of the MSP material, the reaction rates would decrease because the integration of equation (4) is carried out in a smaller wavelength band of the solar flux. Also, the case of a more transparent material the ionization and photodetachment reaction would be reduced, because the corresponding cross sections are smaller. Reduced photoreaction rates would result in a reduced number density of positively charged particles. The less effective photodetachment of negatively charged particles would result in a growth of their abundance during daytime. The effects would change vice versa in case of a more opaque MSP material. Besides, equation (4) represents a classical description of a quantum physical process. For an adequate representation of MSP photo processes laboratory measurements of photoelectrical properties of nanoparticles (MSP analogs) and an in-depth quantum mechanical treatment of these processes are needed, but clearly beyond of this paper.

It also has to be noted that the magnitude of the effect shown here strongly depend on the number density of the MSPs. When decreasing the number of MSPs, the effects shown above should scale correspondingly. But when increasing the number of MSPs within the *D* region there will be a distinct saturation effect, i.e., when all free electrons attach to the MSPs. Beyond sich large MSP number densities, a further increase of the MSP number density would not lead to any additional change of the ionosphere.

In addition, this study represents the quiet ionosphere at auroral latitudes. In the presence of additional ionization due precipitation of energetic electrons and protons we expect that the number densities of positively and negatively charged MSPs would rise. Additional positive MSPs would be produced due to secondary electron emission induced by the precipitating electrons and protons. Also, the number density of negatively charged MSPs would be enhanced due to the attachment of the additional free electrons during the elevated ionization period. This is because the MSP photo reactions are not affected by disturbed ionospheric conditions leading to a steady state at higher negative MSP number density.

For a more quantitative analysis of these uncertainties numerous sensitivity studies with the model are necessary. This is beyond the scope of this study and will be presented in a future paper.

4. Conclusions

Aerosol particles from meteoric origin play an important role within the mesosphere and *D* region ionosphere. This study has shown that MSPs not only have an impact on the charge balance but also alter the quiet *D* region ion chemistry. This has been demonstrated by implementing MSPs as an active component into the reaction scheme of the SIC model. MSP size dependent plasma attachment reactions as well as photo detachment of negatively charged MSP and photoionization of neutral MSPs are the reactions which connect MSP to the standard ion chemistry.

We have identified that the MSPs mainly affect the ion chemistry indirectly via the MSP induced changes of the electron density. During nighttime, electrons effectively attach to the neutral smoke between 80 and 100 km altitude, this process reduces the number of free electrons. Hence, electron-ion recombination occurs less frequently. As a consequence the abundance of positive ions grows, especially water cluster ions ($H^+(H_2O)_n$) can exist in a much higher abundance. This effect of mesospheric aerosols on the abundance of water cluster ions was also discovered by *Gumbel et al.* [2003], albeit for mesospheric ice particles. We demonstrated in this study that also MSPs have an influence on the ion chemistry. This influence is not only limited to the cold summer mesopause but also present during other seasons and altitudes. The much higher abundance of heavy water cluster ions might also be important in the formation of nighttime Polar Mesospheric Winter Echoes at altitudes above 80 km [e.g., *La Hoz and Havnes*, 2008].

Primary negative ions (O_2^-) and many of the secondary negative ions (e.g., (Cl^-) behave similarly as the electron density, i.e., an overall reduction is observed between 60 to 90 km. On the contrary heavier ions, respectively, ions which are formed after several ion-ion reactions, i.e., $Cl^-(HCl)$, are so long lived that attachment to MSPs is an important loss process. The attachment to neutral MSPs and the recombination with charged MSPs occurs especially at lower altitudes below 80 km. This is the case for both, negative as well as positive ions.

During daytime the *D* region chemistry is also changed via the MSP influence on the electron density. In this case, electrons still attach to neutral MSPs but these electrons of the charged MSPs are easily photodetached by sunlight. As a consequence the positive ion chemistry is only sparsely influenced. At lower altitudes it can even occur that ionized MSPs can survive at reasonable number densities of hundreds per cubic centimeter. Hence, the electron density is enhanced here and causes an increase of short-lived negative ions (O_2^-, (Cl^-)) and a reduction of positive water clusters due to enhanced electron-positive ion recombination. The behavior of the long-lived species $Cl^-(HCl)$ is different as it is similarly reduced during nighttime. That indicates again that the attachment to MSPs is an important loss process.

At this point it has to be noted that the composition and microphysical properties of MSPs are still not well known and demand further in situ research as well as laboratory work. Both are important parameters within our model study and need to be quantified in order to enable better model comparisons with ionospheric measurements.

To achieve that goal, we propose incoherent scatter radar (ISR) measurements of the *D* region electron density during sunset and sunrise. Unfortunately, not all ISRs are capable of measuring the very low electron density in the *D* region in the order of several 100 cm^{-3}, which we expect at altitudes below 90 km. The above mentioned drop in electron density at a certain solar zenith angle is a signature for the existence of MSPs in the *D* region and might be detachable only by the Arecibo ISR when observing on a regular basis. We already conducted model simulations for Arecibo conditions and the results are qualitatively similar to the here presented ones. We have also screened the MADRIGAL database (www.openmadrigal.org) for upper atmospheric science for *D* region electron density measurements, which also contains the data of the Arecibo radar. Unluckily, the MADRIGAL database does not provide electron density measurements of the *D* region in a quality that enable extensive *D* region electron density comparisons with the SIC model considering MSP effects. We think that dedicated measurements of the electron density conducted during sunrise and sunset would make it possible to identify such an MSP effect and prove the existence of negatively charged MSPs. Especially the equatorial ionosphere with its sharper day to night transition would be a good subject of investigation to observe this effect.

These electron density measurements then has to be compared to dedicated SIC-modeled electron densities for the Arecibo site. Additional model restrictions, as the characterization of the background atmosphere by satellite measurements are necessary to make reliable statements on the conditions of the lower ionosphere

with our model, i.e., nitric oxide, ozone profiles, and temperature. This radar study would make it also possible to characterize the charging efficiency $\gamma_{charging}$ (see equation (2)) which is a crucial parameter within this study. This parameter is still not very well known but governs how severe the nighttime drop in electron density is.

Acknowledgments
All data used to achieve the presented results can be requested from the corresponding author at carsten.baumann@dlr.de. The authors would like to thank Martin Friedrich for very fruitful discussions on the comparison of our results with data from the Arecibo radar. A.K. was supported by the European Regional Development Fund (Regional Council of Lapland, decision A70179). P.T.V. was supported by the Academy of Finland through the project #276926 (SECTIC: Sun-Earth Connection Through Ion Chemistry).

References

Arnold, F., and D. Krankowsky (1971), Negative ions in the lower ionosphere: A comparison of a model computation and a mass-spectrometric measurement, *J. Atmos. Terr. Phys.*, *33*, 1693–1702.

Asmus, H., S. Robertson, S. Dickson, M. Friedrich, and L. Megner (2015), Charge balance for the mesosphere with meteoric dust particles, *J. Atmos. Sol. Terr. Phys.*, *127*, 137–149, doi:10.1016/j.jastp.2014.07.010.

Baumann, C., M. Rapp, A. Kero, and C.-F. Enell (2013), Meteor smoke influences on the D-region charge balance: Review of recent in situ measurements and one-dimensional model results, *Ann. Geophys.*, *31*(11), 2049–2062, doi:10.5194/angeo-31-2049-2013.

Ferguson, E. E. (1979), Ion-molecule reactions in the atmosphere, in *Kinetics of Ion-Molecule Reactions, NATO Adv. Study Inst. Ser.*, vol. 40, edited by P. Ausloos, pp. 377–403, Springer, New York, doi:10.1007/978-1-4613-2931-2-18.

Friedrich, M., and M. Rapp (2009), News from the lower ionosphere: A review of recent developments, *Surv. Geophys.*, *30*, 525–559.

Friedrich, M., M. Rapp, T. Blix, U.-P. Hoppe, K. Torkar, S. Robertson, S. Dickson, and K. Lynch (2012), Electron loss and meteoric dust in the mesosphere, *Ann. Geophys.*, *30*, 1495–1501, doi:10.5194/angeo-30-1495-2012.

Gumbel, J., D. E. Siskind, G. Witt, K. M. Torkar, and M. Friedrich (2003), Influences of ice particles on the ion chemistry of the polar summer mesosphere, *J. Geophys. Res.*, *108*(D8), 8436, doi:10.1029/2002JD002413.

Hervig, M. E., L. L. Gordley, L. E. Deaver, D. E. Siskind, M. H. Stevens, J. M. Russell, S. M. Bailey, L. Megner, and C. G. Bardeen (2009), First satellite observations of meteoric smoke in the middle atmosphere, *Geophys. Res. Lett.*, *36*, L18805, doi:10.1029/2009GL039737.

Hervig, M. E., L. E. Deaver, C. G. Bardeen, J. M. Russell III, S. M. Bailey, and L. L. Gordley (2012), The content and composition of meteoric smoke in mesospheric ice particles from SOFIE observations, *J. Atmos. Sol. Terr. Phys.*, *84–85*, 1–6, doi:10.1016/j.jastp.2012.04.005.

Hunten, D. M., R. P. Turco, and O. B. Toon (1980), Smoke and dust particles of meteoric origin in the mesosphere and stratosphere, *J. Atmos. Sci.*, *37*, 1342–1357.

Kazil, J. (2002), The University of Bern Atmospheric Ion Model: Time-dependent ion modeling in the stratosphere, mesosphere, and lower thermosphere, PhD thesis, Univ. of Bern, Switzerland.

Kazil, J., E. Kopp, S. Chabrillat, and J. Bishop (2003), The University of Bern Atmospheric Ion Model: Time-dependent modeling of the ions in the mesosphere and lower thermosphere, *J. Geophys. Res.*, *108*(D14), 4432, doi:10.1029/2002JD003024.

La Hoz, C., and O. Havnes (2008), Artificial modification of polar mesospheric winter echoes with an rf heater: Do charged dust particles play an active role?, *J. Geophys. Res.*, *113*, D19205, doi:10.1029/2008JD010460.

Lau, Y. K., S. Ikuta, and P. Kebarle (1982), Thermodynamics and kinetics of the gas-phase reactions $H_3O^+(H_2O)_{n-1} + H_2O = H_3O^+(H_2O)_n$, *J. Am. Chem. Soc.*, *104*(6), 1462–1469, doi:10.1021/ja00370a002.

Megner, L., and J. Gumbel (2009), Charged meteoric particles as ice nuclei in the mesosphere: Part 2. A feasibility study, *J. Atmos. Sol. Terr. Phys.*, *71*, 1236–1244, doi:10.1016/j.jastp.2009.05.002.

Megner, L., M. Rapp, and J. Gumbel (2006), Distribution of meteoric smoke—Sensitivity to microphysical properties and atmospheric conditions, *Atmos. Chem. Phys.*, *6*, 4415–4426, doi:10.5194/acp-6-4415-2006.

Megner, L., D. E. Siskind, M. Rapp, and J. Gumbel (2008), Global and temporal distribution of meteoric smoke: A two-dimensional simulation study, *J. Geophys. Res.*, *113*, D03202, doi:10.1029/2007JD009054.

Mitra, A. (1981), Chemistry of middle atmospheric ionization—A review, *J. Atmos. Terr. Phys.*, *43*(8), 737–752, doi:10.1016/0021-9169(81)90050-7.

Narcisi, R. S., and A. D. Bailey (1965), Mass spectrometric measurements of positive ions at altitudes from 64 to 112 kilometers, *J. Geophys. Res.*, *70*(15), 3687–3700, doi:10.1029/JZ070i015p03687.

Natanson, G. L. (1960), On the theory of the charging of atmospheric aerosol particles as a result of capture of gas ions, *Sov. Phys. Tech. Phys.*, *5*, 538–551.

Pavlov, A. (2014), Photochemistry of ions at D-region altitudes of the ionosphere: A review, *Surv. Geophys.*, *35*(2), 259–334, doi:10.1007/s10712-013-9253-z.

Phelps, A. (1969), Laboratory studies of electron attachment and detachment processes of aeronomic interest, *Can. J. Chem.*, *47*(10), 1783–1793.

Picone, J. M., A. E. Hedin, D. P. Drob, and A. C. Aikin (2002), NRLMSISE-00 empirical model of the atmosphere: Statistical comparisons and scientific issues, *J. Geophys. Res.*, *107*(A12), 1468, doi:10.1029/2002JA009430.

Plane, J. M. C., et al. (2014), A combined rocket-borne and ground-based study of the sodium layer and charged dust in the upper mesosphere, *J. Atmos. Sol. Terr. Phys.*, *118*, 151–160, doi:10.1016/j.jastp.2013.11.008.

Plane, J. M. C., W. Feng, and E. C. M. Dawkins (2015), The mesosphere and metals: Chemistry and changes, *Chem. Rev.*, *115*(10), 4497–4541, doi:10.1021/cr500501m.

Rapp, M. (2000), Capture rates of electrons and positive ions by mesospheric aerosol particles, *J. Aerosol Sci.*, *31*, 1367–1369.

Rapp, M. (2009), Charging of mesospheric aerosol particles: The role of photodetachment and photoionization from meteoric smoke and ice particles, *Ann. Geophys.*, *27*, 2417–2422, doi:10.5194/angeo-27-2417-2009.

Rapp, M., and F.-J. Lübken (2001), Modelling of particle charging in the polar summer mesosphere: Part 1—General results, *J. Atmos. Sol. Terr. Phys.*, *63*(8), 759–770.

Rapp, M., and G. E. Thomas (2006), Modeling the microphysics of mesospheric ice particles: Assessment of current capabilities and basic sensitivities, *J. Atmos. Sol. Terr. Phys.*, *68*, 715–744, doi:10.1016/j.jastp.2005.10.015.

Rapp, M., et al. (2010), Rocket-borne in situ measurements of meteor smoke: Charging properties and implications for seasonal variation, *J. Geophys. Res.*, *115*, D00I16, doi:10.1029/2009JD012725.

Rapp, M., J. M. C. Plane, B. Strelnikov, G. Stober, S. Ernst, J. Hedin, M. Friedrich, and U.-P. Hoppe (2012), In situ observations of meteor smoke particles (MSP) during the Geminids 2010: Constraints on MSP size, work function and composition, *Ann. Geophys.*, *30*, 1661–1673, doi:10.5194/angeo-30-1661-2012.

Robertson, S., S. Dickson, M. Horanyi, Z. Sternovsky, M. Friedrich, D. Janchez, L. Megner, and B. Williams (2013), Detection of meteoric smoke particles in the mesosphere by a rocket-borne mass spectrometer, *J. Atmos. Sol. Terr. Phys.*, *118*, 161–179, doi:10.1016/j.jastp.2013.07.007.

Rosinski, J., and R. H. Snow (1961), Secondary particulate matter from meteor vapors, *J. Meteorol.*, *18*, 736–745.

Schulte, P., and F. Arnold (1992), Detection of upper atmospheric negatively charged microclusters by a rocket-borne mass spectrometer, *Geophys. Res. Lett.*, *19*, 2297–2300.

Strelnikova, I., M. Rapp, S. Raizada, and M. Sulzer (2007), Meteor smoke particle properties derived from Arecibo incoherent scatter radar observations, *Geophys. Res. Lett.*, *34*, L15815, doi:10.1029/2007GL030635.

Tobiska, W. K., and S. D. Bouwer (2006), New developments in SOLAR2000 for space research and operations, *Adv. Space Res.*, *37*(2), 347–358, doi:10.1016/j.asr.2005.08.015.

Turunen, E., H. Matveinen, J. Tolvanen, and H. Ranta (1996), D-region ion chemistry model, in *STEP Handbook of Ionospheric Models*, edited by R. W. Schunk, pp. 1–25, SCOSTEP Secretariat, Boulder, Colo.

Verronen, P. T. (2006), Ionosphere-atmosphere interaction during solar proton events, PhD thesis, Univ. of Helsinki, Helsinki. [Available at http://urn.fi/URN:ISBN:952-10-3111-5.]

Verronen, P. T., A. Seppälä, M. A. Clilverd, C. J. Rodger, E. Kyrölä, C.-F. Enell, T. Ulich, and E. Turunen (2005), Diurnal variation of ozone depletion during the October-November 2003 solar proton events, *J. Geophys. Res.*, *110*, A09S32, doi:10.1029/2004JA010932.

Vostrikov, A., and D. Dubov (2006a), Absolute cross sections of electron attachment to molecular clusters: Part I. Formation of $(CO_2)_N^-$, *Tech. Phys.*, *51*(5), 540–547, doi:10.1134/S1063784206050021.

Vostrikov, A., and D. Dubov (2006b), Absolute cross sections of electron attachment to molecular clusters. Part II: Formation of $(H_2O)_N^-$, $(N_2O)_N^-$, and $(N_2)_N^-$, *Tech. Phys.*, *51*(12), 1537–1552, doi:10.1134/S1063784206120012.

Winkler, H., S. Kazeminejad, M. Sinnhuber, M.-B. Kallenrode, and J. Notholt (2009), Conversion of mesospheric HCl into active chlorine during the solar proton event in July 2000 in the northern Polar Region, *J. Geophys. Res.*, *114*, D00I03, doi:10.1029/2008JD011587.